Acknowledgements: This work was supported by the Director, Office of Science, Office of Basic Energy Sciences, Material Sciences and Engineering Division, of the U.S. Department of Energy under Contract No. DE-AC02-05CH11231. We thank the National Center for Electron Microscopy for the use of their facilities.

Direct Photonic–Plasmonic Coupling and Routing in Single Nanowires

Ruoxue Yan, Peter Pausauskie, Jiaxing Huang, Peidong Yang

Department of Chemistry, University of California, Berkeley; Materials Sciences Division, Lawrence Berkeley National Laboratory, Berkeley, CA 94720

Metallic nanoscale structures are capable of supporting surface plasmon polaritons (SPPs) –propagating collective electron oscillations with tight spatial confinement at the metal surface. SPPs represent one of the most promising structures to beat the diffraction limit imposed by conventional dielectric optics. Ag nanowires have drawn increasing research attention due to two-dimensional sub-100nm mode confinement and lower losses as compared to fabricated metal structures. However, rational and versatile integration of Ag nanowires with other active and passive optical components, as well as Ag nanowire based optical routing networks has yet to be achieved. Here, we demonstrate that SPPs can be excited simply by contacting a silver nanowire with a SnO_2 nanoribbon that serves both as an unpolarized light source and a dielectric waveguide. The efficient coupling makes it possible to measure the propagation-distance dependent waveguide spectra and frequency-dependent propagation length on a single Ag nanowire. Furthermore, we have demonstrated prototypical photonic-plasmonic routing devices, which are essential for incorporating low-loss Ag nanowire waveguides as practical components into high capacity photonic circuits.

Recent research efforts have scaled down the plasmonic waveguides[1-6] from

microscale metal stripes[7] to nanoparticles arrays[8, 9] and nanowires[4-6, 10-12], demonstrating the feasibility of sub-wavelength plasmonic optics. However, the inherent metal loss makes it impractical to transfer digital data across the entire photonic IC chip (~1mm) solely with plasmonic waveguides. It becomes increasingly important to be able to integrate plasmonic modules with low-loss, dielectric optical interconnects. In order to achieve such hybrid plasmonic-photonic circuit, it is critical to develop nanoscale plasmonic waveguides with reduced losses and small mode volume, and equally important, to ensure the compatibility with conventional optical circuitry. In this context, chemically synthesized Ag nanowires have emerged as promising candidates for sub-wavelength plasmonic waveguides. The high crystallinity and atomically smooth surface of Ag nanowires should reduce the total propagation loss as compared to those microfabricated polycrystalline Ag waveguides. As a result, Ag nanowires are able to support surface plasmon propagation with two-dimensional subwavelength mode confinement. However, integrating the low-loss Ag nanowire waveguides into a plasmonic-photonic routing network requires a simple, efficient and versatile strategy to couple the light field in and out of the Ag nanowire so that the digital information can be launched and harvested.

The major challenge in optically exciting SPPs in Ag nanowires lies in the dispersion relation mismatch for SPPs and photons. To bridge the difference in the wave vector k_x along the propagation direction $\vec{x}$, at any given photon energy $\hbar\omega$, the photon momentum $\hbar k_x$ ($=\hbar\omega/c\sqrt{\varepsilon_0}$, ε_0 being the dielectric constant of the dielectric enviroment) has to increase by a $\hbar\Delta k_x$ in order to couple photons into SPPs. Various methods have been proposed to bridge this gap and launch propagating SPPs in Ag nanowires. The total internal reflection (TIR) illumination method utilizes a prism to match the momentum

of SPPs and the incident photons[5, 12]. Direct local excitation was demonstrated by focusing a laser on the end facets of the Ag nanowires[6] or on a metallic nanoparticle attaching to the surface of the Ag nanowire that act as a scattering center[13]. A quantum emitter in the near-field of a Ag nanowire can excite propagating SPPs as the optical dipolar near-field contains large momentum components matching those of SPPs[14, 15]. However, these coupling schemes do not lead to easy interconnection with conventional optical components for photonic IC fabrication. The recently reported polymer-Ag coupling method is an important advance towards on-chip integration. However, it still has many restrictions on the coupling conditions, including Ag nanowire orientation, position and incident light field polarization[16].

Here we propose a simple approach to couple SPPs into the Ag nanowires with an inorganic dielectric nano-waveguide – SnO_2 nanoribbon. Single-crystalline SnO_2 nanoribbon have been established as efficient UV-NIR waveguides[17-19]. Their high aspect ratio, strength and flexibility enable their manipulation on surfaces, and can be assembled into optical networks and components. SnO_2 nanoribbons also exhibit photoluminescence with UV excitation and can act as a simultaneous nanoscale light source and waveguide. The Ag nanowires used in this work was synthesized by a modified polyol synthesis. The nanowires have 5 folding twinning planes along their axis, and they are bound by 5 atomically smooth single crystalline {100} surfaces. We demonstrate that Ag nanowire SPPs can be excited by simply contacting with a SnO_2 nanoribbon with minimum restriction on the coupling conditions. SPPs can be launched into the Ag nanowire at arbitrary positions at any orientation. The assembly of the metal-dielectric junction is completely reversible, making it possible to monitor the properties of a single Ag nanowire while varying the interconnection and propagation condition. This versatile coupling strategy represents a major step towards realizing photonic-plasmonic hybrid circuitry and has made possible the systematic far-field study on the SPP propagation

in Ag nanowires.

Results and Discussion

Figure 1a illustrates schematically the device setup. A silver nanowire sits on top of a SnO_2 nanoribbon waveguide that bridges two oxidized Si substrates. A UV laser was focused on the lower right corner of a SnO_2 nanoribbon to excite the broad-band photoluminescence (PL) of SnO_2, which is then waveguided along the nanoribbon towards the Ag nanowire. At the metal-dielectric boundary, photons travelling in the SnO_2 waveguide are scattered with a broad distribution of wave vectors and offer the Δk_x needed to match the momentum of photons and SPPs. The SPPs are guided within the 100nm Ag nanowires and scatter back into free space photons at the distal ends of the wire. Figure 1b is a microscope PL image of the real device built according to the schematics in Figure 1a. A SnO_2 ribbon ($n=2.1$) rests horizontally in the image, bridging a trench between two Si substrates (not shown) with 500nm thermal oxide ($n=1.45$). The bright white PL of the nanoribbon was excited from the far right end of the ribbon with a 325 nm He:Cd laser and while the photons are waveguided along the ribbon, they scattered off the local defects and other scatter centers, outlining the profile of the ribbon in the PL image. The bright white scattering spot is the metal-dielectric junction and the end emissions from the 20μm long, 100nm diameter Ag nanowire appearing in the image as a green spot on the lower left and a red spot on the upper right side of the ribbon. Both the Ag nanowire and the SnO_2 ribbon were positioned with a triple-axis micromanipulator equipped with a tungsten probe under a dark-field microscope. The Scanning Electron Microscope (SEM) image of the device is shown in Figure 1c.

When squeezing the propagating SPPs into a highly confined geometry like a 100nm Ag nanowire, one central question is how the SPP propagation

properties are modified compared to the bulk and other less confined geometries. One phenomenon that has been well-known for metal films[20] and metal micro-strips[21] is a frequency dependent propagation loss. The attenuation of the electromagnetic field along the propagation direction arises from two sources: the *radiative* and *non-radiative loss*. The radiative loss is attributed to back-coupling of SPPs into photons, and is characteristic for asymmetric two-interface systems, as with TIR coupled devices[20]. Non-radiative loss, on the other hand, is due to absorption within the metal owing to the finite conductance of metal at optical frequencies. This is the dominant contribution to our system where the Ag nanowire is in a symmetric dielectric environment. The non-radiative loss depends on the dielectric function of the oscillation frequency of the SPPs. As the frequency of the incident photon decreases from visible to the near infra-red (NIR), the real part of the Ag dielectric constant ($\mathrm{Re}\{\varepsilon_{Ag}\}<0$) becomes more negative, while the imaginary part $\mathrm{Im}\{\varepsilon_{Ag}\}$ remains roughly constant. As a result, the electromagnetic field decays faster inside the metal, thus less metal absorption or Joule heating is expected.

For the Ag nanowires studied here, the frequency dependence of SPP propagation loss is clearly observed, as indicated by the color difference in the end emissions from the Ag nanowire in Figure 1b. As the distance of SPP propagation (d_p), defined here by the distance between the silver wire tips and the coupling point on the SnO_2 ribbon, increases, the high-frequency components damp faster than the low frequency ones, so the frequency distribution of the SPPs is expected to red-shift with increasing d_p. Here, the left silver end-facet is just 3μm from the SnO_2 ribbon, while the right end-facet is more than 10μm from the SPP launching point, thus more red-components are expected from the right emission end-facet, as observed in the experiment.

To further confirm the frequency-dependence of the propagation loss in Ag nanowires, we measured the tip emission spectra from a single Ag nanowire as a function of d_p and compared them to the SnO_2 ribbon emission which serves as the input signal. Using the triple-axis micromanipulator, we were able to pick the Ag nanowire up from the SnO_2 ribbon, move it along the original orientation of the Ag nanowire, and put it back on the SnO_2 ribbon, so that different segments of the Ag nanowire came in contact with the SnO_2 waveguide. The true-color image of the device (Figure 2a) and corresponding spectrum of the tip emission (Figure 2b) were recorded at each position. Great care was taken to make sure that d_p was the only variable in the setup with the orientation of the Ag nanowire unchanged when the Ag nanowire was moved to a new position. Also, the particular position on the SnO_2 ribbon used for coupling was chosen to be free from large scattering centers that would increase background scattering signals.

The color images (collected with a 60x Olympus objective and a true color camera) in Figure 2a show a gradual change in the Ag nanowire tip emission colors from yellow, which is very close to the PL of the particular ribbon used here, to orange, and finally red when the distance of propagation, d_p, from the coupling point to the wire tip increased from 1.5μm to 3.0μm and 9.9μm. Figure 2b compares the spectra of both the SnO_2 ribbon PL emission, which is the input signal, to the tip emission spectra corresponding to the images in Figure 2a. The input PL spectra taken from the tip of the SnO_2 ribbon was a smooth Gaussian peak extend from 400nm to 800nm and with the maximum at 590nm. The tip emission spectrum for the lowest d_p =1.5μm resembles the input spectrum generally, but already starts to show a steep slope at the high frequency side of the peak, a red-shift of the left intensity-cutoff wavelength to 430nm, as well as a slight red-shift of the peak position, indicating an attenuation at the high frequency end. The red shift of the peak position was more prominent for the tip spectra for longer d_ps, with the emission maximum

at ~620nm for d_p =3.0μm, and ~670m for d_p =9.9μm. The red-shift of the intensity-cutoff wavelength on the high-frequency side was also significant at these longer d_ps. For d_p =3.0μm, the intensity-cutoff was at ~440nm and was at ~510nm for d_p =9.9μm, a red-shift of more than 100nm compared to the input spectrum. All these signs clearly demonstrate a much smaller propagation loss as the frequency decreases.

In a metal waveguide, the internal damping of SPP propagating away from the excitation along the propagation direction, $\vec{x}$, decreases exponentially as $I=I_0 e^{-x/L}$. L, the propagation length, is defined by the characteristic length after which the intensity decreases to 1/e and is a measure of the propagation loss at a given frequency. L is determined by the imaginary part of the complex plasmon wave vector k_x, given by $L = \frac{1}{2\mathrm{Im}[k_x]}$. To quantitatively measure the propagation length in our Ag nanowires, we designed an experimental setup illustrated in Figure 3a. Similar to the coupling device used before, a SnO_2 nanoribbon was used to excite the SPP propagation in the Ag nanowire, but here the input signal was no longer the broad-band PL of SnO_2. Fixed to the tapered tip of an optical fiber coupled to the visible and NIR lasers, a SnO_2 nanoribbon served as a dielectric waveguide to deliver laser photons to the Ag nanowire. This probe made of a SnO_2 nanoribbon and an optical fiber was then mounted on a micromanipulator with a ~15° angle to the focus plane of a dark-field microscope and is capable of scanning in three directions with 0.1μm resolution. Figure S1a shows a dark field image of the probe when the tip of the SnO_2 nanoribbon was brought into focus. This probe was then brought into contact with a Ag nanowire sitting on the edge of an oxidized Si substrate.

Figure 3a and S1 illustrate how this setup was used for the propagation length

measurement. As the SnO_2 - Ag junction was moved towards the tip of the Ag nanowire, the distance for which the SPP modes had to travel before scattering back into photons at the end-facet of the Ag nanowire (d_p) decreased, and the tip emission intensity (I) increased accordingly. If we assume 1) the tip emission intensity was proportional to the intensity of the propagating SPPs modes, and 2) the dielectric-metal coupling efficiency remains constant as the SnO_2 nanoribbon was sliding on the Ag nanowire, the only variable in the process was d_p. We can estimate in this way the propagation length (L) from the slope of the $\ln(I)$- d_p plot. Here it should be noted that our assumption of the constant coupling efficiency is based on the fact that the probe can glide along the perpendicular Ag nanowire without bending the wire, moving the coupling point on the probe or disturbing the coupling angle, as shown in Figure S1b-f.

Figure 3b gives the typical $\ln(I)$- d_p plots for 3 wavelength: 532nm, 650nm and 980nm. The propagation length calculated from the slop of the plots shows strong frequency dependence, increasing from 6.2μm for 532nm, to 11.3μm for 650nm and finally to 20.2μm for 980nm IR excitation. And the standard deviations from different wires were less than 0.4μm. This result agrees well with the frequency dependence we observed in the case of broad-band excitation. The trend of increasing propagation length with wavelength agrees well with the result from fabricated Ag microstrips[21] and extends to the telecommunication wavelength, according to the dispersion relation of the surface plasmon modes for a 100nm metal cylinder in vacuum[22].

The propagation length sets the upper size limit for any plasmonic feature on a photonic circuit. Another characteristic length, the decay length of electric field in surrounding dielectric environment, δ_d, which is typically on the order of half of the wavelength of light involved, dictates the maximum distance between any plasmonic or dielectric features that can have overlapping modes

and couple to one another. Inter-wire coupling has been previous observed in a random assembly of Ag nanowires[6]. However, a rational integration of dielectric and Ag nanowire waveguide components into optical-plasmonic routing devices, which is essential to incorporating Ag nanowire waveguides as practical components into highly integrated photonic circuits, is yet to be demonstrated.

Here, both dielectric-metal-metal (DMM) and dielectric-metal-dielectric (DMD) coupling devices were designed and assembled to demonstrate the feasibility of optical-plasmonic routing. The device structure was illustrated in the SEM image in Figure 4a, showing a silver nanowire sitting on top of a SnO_2 ribbon, with a second silver nanowire attached to it with a 12μm overlap. The colored arrows points to the tips of the nanowires and the magnified image of the Ag nanowire junction is given in the inset. The surfactants on the Ag nanowires have been removed so that the two Ag nanowires were in direct contact. Figure 4b and 4c show the intensity map and true-color image of the routing of SnO_2 ribbon PL. SPPs are launched into the first Ag nanowire at the metal (Ag)-dielectric (SnO_2) junction, and coupled into the second one evanescently without scattering loss along the metal-metal junction. They were scattered back into photons at the 3 discontinuities (wire tips) along the propagation direction, as marked by the color arrows whose positions are in accordance with Figure 4a. Despite the radiative losses at the wire tips, the SPP modes are able to propagate without complete attenuation to the farthest tip of the second wire that was 40μm away from the excitation (Ag-SnO_2 junction). This efficient plasmonic coupling between Ag nanowires in this routing device was a comprehensive result of the overlapping k_x, the long Ag-Ag junction, and the large SPP mode overlapping due to the minimum distance between the wires.

It should be noted that the dependence of the tip emission color on d_p in the

single nanowire case is also observed in the coupling device. Figure 4d-f displays the red, green and blue color panel of the true color image in Figure 4c. The closer the tips were to the excitation, their emissions composed more high-frequency components. The blue components only exist at the first Ag nanowire tip that's 8μm from the excitation, while green ones survived 20μm of propagation, and the red ones were the only visible frequencies that were observable at farthest emission point, 40μm from excitation.

The design of the dielectric-metal-dielectric (DMD) coupling device is shown in the dark-field microscope image (Figure 5a). The two SnO_2 nanoribbons lying on an oxidized Si substrate were bridged with an Ag nanowire. The PL of the bent ribbon was excited from hundreds of micrometers away from the Ag-SnO_2 junctions to avoid direct excitation of the straight ribbon. In the absence of the Ag nanowire (Figure5b), the propagating modes of the straight ribbon was not excited, with only a week scattering signal at the tip close to the bent ribbon. However, with the Ag nanowire bridging the two ribbons, the SPPs launched into the Ag nanowire couple back to guided optical modes in the straight ribbon, which then propagate 43μm to the distal end and scatter into free-space photons.

In conclusion, we have demonstrated the coupling between photonic and plasmonic waveguides at the single nanowire level. The frequency dependent propagation loss was observed in Ag nanowire and was confirmed by quantitative measurement and in agreement with theoretical expectations. Rational integration of dielectric and Ag nanowire waveguide components into hybrid optical-plasmonic routing devices has been demonstrated. This capability is essential for incorporating low-loss Ag nanowire waveguides as practical components into high capacity photonic circuits and can be extended to other inorganic dielectric waveguide systems such as Si, SiO_2, GaN, and Si_3N_4.

Materials and Methods:

SnO_2 nanoribbon synthesis: SnO_2 nanoribbon waveguides were synthesized using a chemical vapor transport method previously described[23]. SnO powder was heated in a quartz tube reactor at 1100 ^{0}C under 350 Torr of flowing argon (50 sccm). Milligram quantities of ribbons were collected on an alumina boat near the center of the reactor and deposited onto clean substrates by dry transfer.

Ag nanowire synthesis: The Ag nanowires were synthesized by reducing $AgNO_3$ with Ethylene Glycol (EG) in the presence of Poly(vinyl pyrrolidone) (PVP) [24]. Three stock solutions for the Ag nanowire synthesis were prepared at room temperature by dissolving 50mg NaCl, 50mg $AgNO_3$ and 200mg PVP (50,000g/mol) in 20ml EG, respectively. 50µL $AgNO_3$ solution and 150µL NaCl solution was added to 5ml of PVP solution while stirring at room temperature in a 25ml flask. After 5 minutes, the flask was then transferred to an oil bath at 170-180˚C, heated for ~5 mins till the mixture turned from white to orange, and injected with additional 0.5-2 ml of $AgNO_3$. After heating for 10-15 more minutes, the product was collected and washed with EG and ethanol to remove excess PVP. The purified nanowires were stored in ethanol. The product was then drop-cast on a PDMS substrate for manipulation. The synthesis yield large quantity of nearly pure Ag nanowires with nearly monodispersed diameter (100 nm) and lengths up to 50 µm.

Optical Characterization:

A HeCd laser (Melles Griot, Irvine, CA) provided unpolarized continuous wave (CW) UV excitation (325 nm) for the photoluminescence of SnO_2 waveguide. CW diode lasers (532 nm, 650nm and 980nm) supplied visible lights for the propagation length measurement. The lasers were either focused to a beam diameter of 50µm on the SnO_2 nanoribbons or coupled to an optical fiber.

Intensity maps and color images were recorded with two microscope-mounted cameras (iXon, Andor Technology, Belfast, Northern Ireland and CoolSnap cf, Photometrics, Tucson, AZ). The tip-emission spectra measurement was performed with an inverted microscope (Olympus, IX71). Signal was collected through a 60x microscope objective lens (NA=0.7) and captured by a 1,340x400 pixel, back-illuminated CCD (Princeton Instruments, Spec-10:400B) and spectrometer (Princeton Instruments, SpectraPro 2300i).

Manipulation and Probe fabrication for the propagation length measurement: For nanoribbon manipulation, we used a three-axis commercial micromanipulator equipped with tungsten probes (≈400 nm tip diameter). The probe utilized for exciting the ribbon waveguide was fabricated by attaching a SnO_2 nanoribbon to a chemically-etched[25] multi-mode UV-IR optical fiber with epoxy adhesive.

Acknowledgment. This work was supported by the Director, Office of Science, Office of Basic Energy Sciences, Division of Materials Sciences and Engineering of the U.S. Department of Energy under Contract No. DE-AC02-05CH11231 and NIH.

References:

1. Lal, S., Link, S. & Halas, N.J. Nano-optics from sensing to waveguiding. *Nature Photonics* **1**, 641-648 (2007).
2. Ozbay, E. Plasmonics: Merging photonics and electronics at nanoscale dimensions. *Science* **311**, 189-193 (2006).
3. Barnes, W.L., Dereux, A. & Ebbesen, T.W. Surface plasmon subwavelength optics. *Nature* **424**, 824-830 (2003).
4. Graff, A., Wagner, D., Ditlbacher, H. & Kreibig, U. Silver nanowires. *European Physical Journal D* **34**, 263-269 (2005).
5. Ditlbacher, H. et al. Silver nanowires as surface plasmon resonators. *Phys Rev Lett* **95**, - (2005).
6. Sanders, A.W. et al. Observation of plasmon propagation, redirection, and fan-out in silver nanowires. *Nano Lett* **6**, 1822-1826 (2006).
7. Krenn, J.R. & Weeber, J.C. Surface plasmon polaritons in metal stripes and wires. *Philosophical Transactions of the Royal Society of London Series a-Mathematical Physical and Engineering Sciences* **362**, 739-756 (2004).
8. Maier, S.A. Plasmonics: The promise of highly integrated optical devices. *IEEE J Sel Top Quant* **12**, 1671-1677 (2006).
9. Maier, S.A. et al. Local detection of electromagnetic energy transport below the diffraction limit in metal nanoparticle plasmon waveguides. *Nature Materials* **2**, 229-232 (2003).
10. Krenn, J.R. et al. Non diffraction-limited light transport by gold nanowires. *Europhysics Letters* **60**, 663-669 (2002).
11. Zia, R., Schuller, J.A. & Brongersma, M.L. Near-field characterization of guided polariton propagation and cutoff in surface plasmon waveguides. *Physical Review B* **74**, - (2006).
12. Dickson, R.M. & Lyon, L.A. Unidirectional plasmon propagation in metallic nanowires. *J Phys Chem B* **104**, 6095-6098 (2000).
13. Knight, M.W. et al. Nanoparticle-mediated coupling of light into a nanowire. *Nano Lett* **7**, 2346-2350 (2007).
14. Fedutik, Y., Temnov, V., Woggon, U., Ustinovich, E. & Artemyev, M. Exciton-plasmon interaction in a composite metal-insulator-semiconductor nanowire system. *Journal of the American Chemical Society* **129**, 14939-14945 (2007).
15. Akimov, A.V. et al. Generation of single optical plasmons in metallic nanowires coupled to quantum dots. *Nature* **450**, 402-406 (2007).
16. Pyayt, A.L., Wiley, B., Xia, Y., Chen, A. & Dalton, L. Integration of photonic and silver nanowire plasmonic waveguides. *Nature Nanotechnology* **3**, 660-665 (2008).
17. Law, M. et al. Nanoribbon waveguides for subwavelength photonics integration. *Science* **305**, 1269-1273 (2004).
18. Sirbuly, D.J. et al. Optical routing and sensing with nanowire assemblies. *Proceedings of the National Academy of Sciences of the United States of America* **102**, 7800-7805 (2005).
19. Sirbuly, D.J., Law, M., Yan, H.Q. & Yang, P.D. Semiconductor nanowires for subwavelength photonics integration. *J Phys Chem B* **109**, 15190-15213 (2005).
20. Raether, H. Surface Plasmons on Smooth and Rough Surfaces and on Gratings

(Springer-Verlag, Berlin, Germany; 1988).

21. Lamprecht, B. et al. Surface plasmon propagation in microscale metal stripes. *Applied Physics Letters* **79**, 51-53 (2001).
22. Novotny, L. & Hafner, C. Light-Propagation in a Cylindrical Wave-Guide with a Complex, Metallic, Dielectric Function. *Physical Review E* **50**, 4094-4106 (1994).
23. Pan, Z.W., Dai, Z.R. & Wang, Z.L. Nanobelts of semiconducting oxides. *Science* **291**, 1947-1949 (2001).
24. Sun, Y.G., Yin, Y.D., Mayers, B.T., Herricks, T. & Xia, Y.N. Uniform silver nanowires synthesis by reducing AgNO3 with ethylene glycol in the presence of seeds and poly(vinyl pyrrolidone). *Chemistry of Materials* **14**, 4736-4745 (2002).
25. Haber, L.H., Schaller, R.D., Johnson, J.C. & Saykally, R.J. Shape control of near-field probes using dynamic meniscus etching. *Journal of Microscopy-Oxford* **214**, 27-35 (2004).

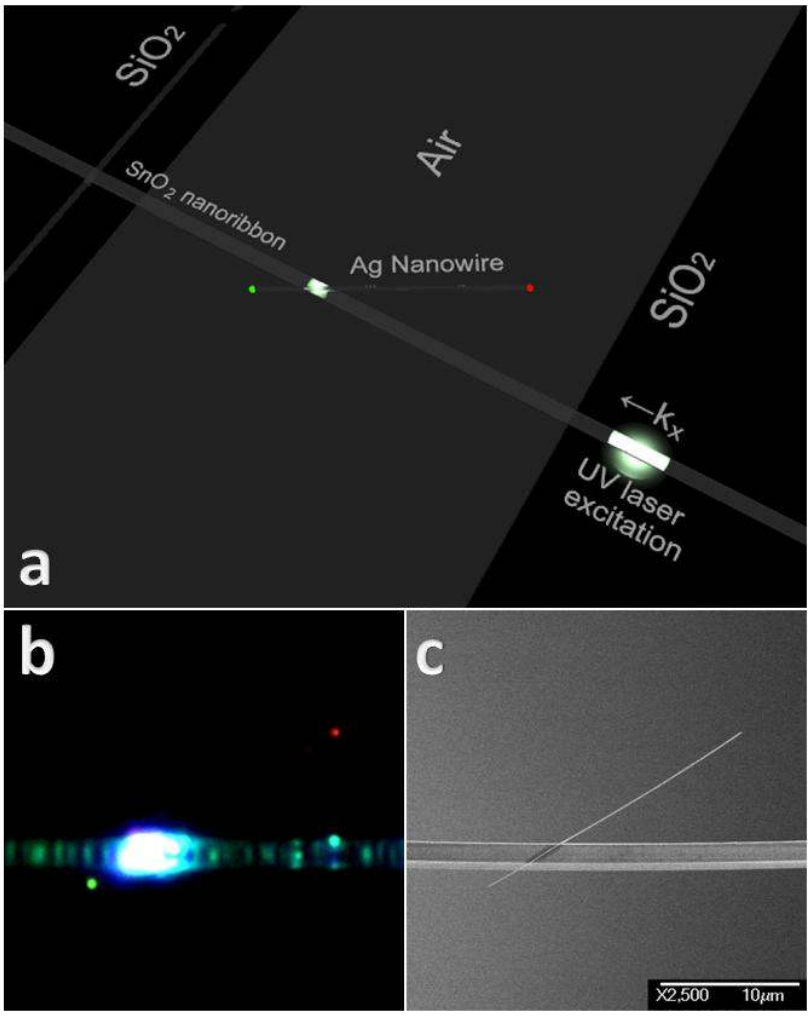

Figure 1 Excitation and propagation of plasmon modes in a Ag nanowire waveguide. **a.** Schematic of the photonic-plasmonic routing device showing a Ag nanowire/SnO_2 nanoribbon cross-junction structure suspended between two SiO2/Si wafers. A UV laser beam was focused on the lower right part of the SnO_2 nanoribbon to excite its self-guided broad band photoluminescence (PL). Light scattered at the metal-dielectric junction was coupled into surface plasmon modes of the Ag nanowire, which was waveguided to propagate along the wire and finally scattered back into free space photon at the two distal ends. **b,** Optical microscope image of the actual photonic-plasmonic routing device illustrated in **a.** The emission (green and red) from both tips of the Ag nanowire can be observed by eye. The SnO_2 nanoribbon was excited from the far right section (not shown). Scale bar is 20μm **c,** SEM image of the same device in **b**.

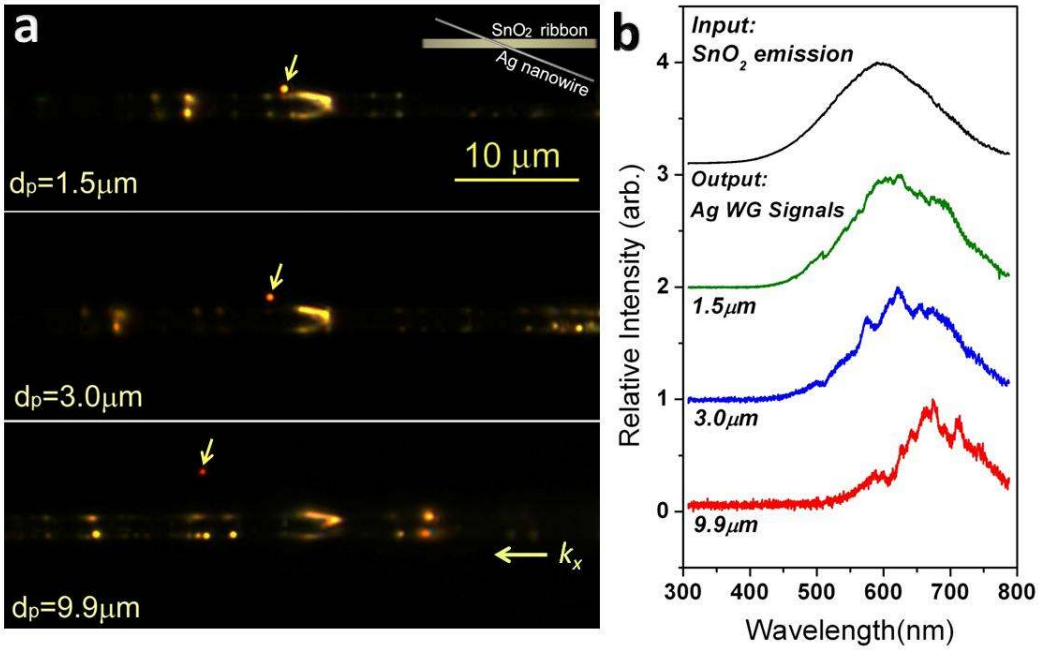

Figure 2 Dependence of Ag nanowire waveguide spectra on the propagation distance (d_p). a, True color optical microscope images showing Ag nanowire/SnO_2 nanoribbon junctions of different propagating distance fabricated by micromanipulation. The coupling angle of the Ag/SnO_2 junction was kept constant. The color of the end emission from the Ag nanowire contained more red-components with increasing d_p. The schematic of the setup is shown in the inset at the upper right corner. **b,** Emission spectra of the Ag nanowire corresponding to the images in **a**, and the PL spectrum of the SnO_2 ribbon (input signal) used in the experiment.

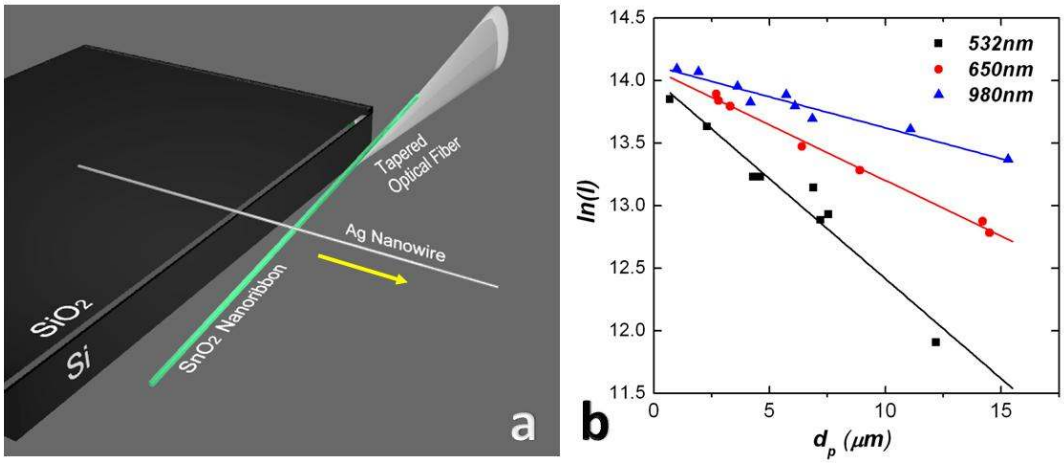

Figure 3 Frequency dependence of Ag nanowire SPP propagation length (*L*). a, Schematic of the experimental setup for measuring propagation length. A Ag nanowire is sitting on the edge of a thermal oxide substrate. Lasers of different frequencies were coupled into the Ag nanowire through a scanning SnO_2 nanoribbon probe attached to the end of an optical fiber. The yellow arrow indicates the sliding direction of the nanoribbon probe. **b,** Plot of *ln(Intensity)* as a function of propagation distance d_p at 2 visible wavelengths: **532nm** (green) and **650nm** (red); and an IR wavelength: **980nm**. The propagation lengths for the 3 wavelengths were 6.2μm, 11.3μm and 20.2μm, respectively.

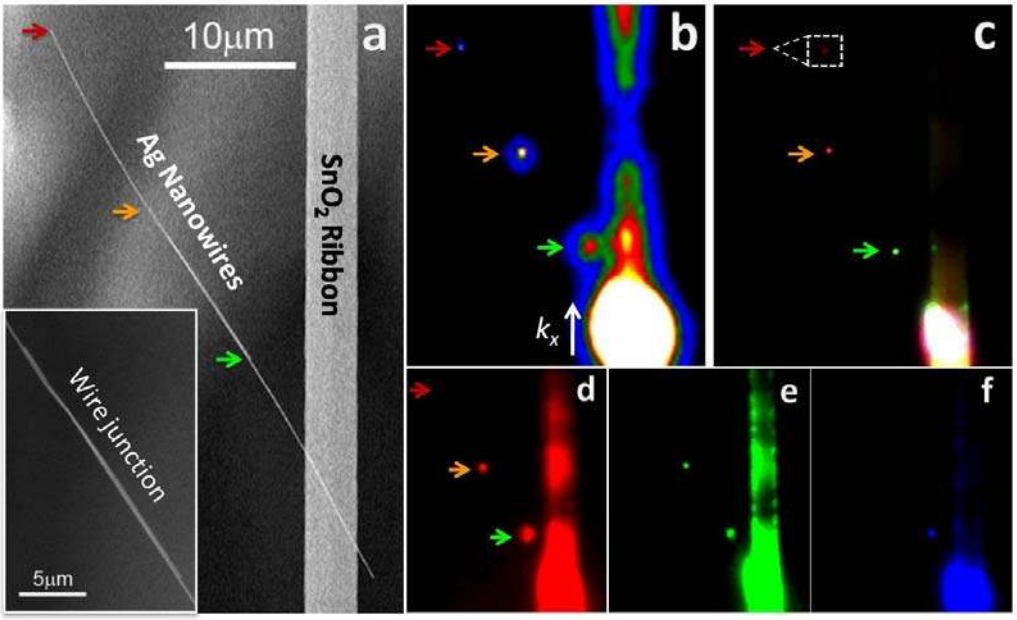

Figure 4 Dielectric-metal-metal (D-M-M) optical routing. a, SEM image of the D-M-M routing structure, showing a pair of overlapping silver nanowires couple to a SnO_2 ribbon. The overlapping length of the two Ag nanowires was12μm. The inset shows the overlapping section of the two metal nanowires. The end of Ag nanowire-1 was marked by the orange arrow. The tips of Ag nanowire-2, which was not in direct contact with the ribbon were marked with the green and red arrows. **b,** Intensity map of the routing device when the PL of the SnO2 ribbon was excited from far below (out of scope) and coupled into nanowire-1 that's in direct contact with the ribbon and then propagate to nanowire-2, showing 3 distinct emission points at the 3 distal ends of the nanowires. **c,** The true color image of the same view as in **b**, the emission from the far end of nanowire-2 shown in the white dotted box was brought out by adjusting brightness of the area. **d-f,** the red, green and blue panels of **c**, showing a systematic decrease in propagation loss from blue to red optical frequencies.

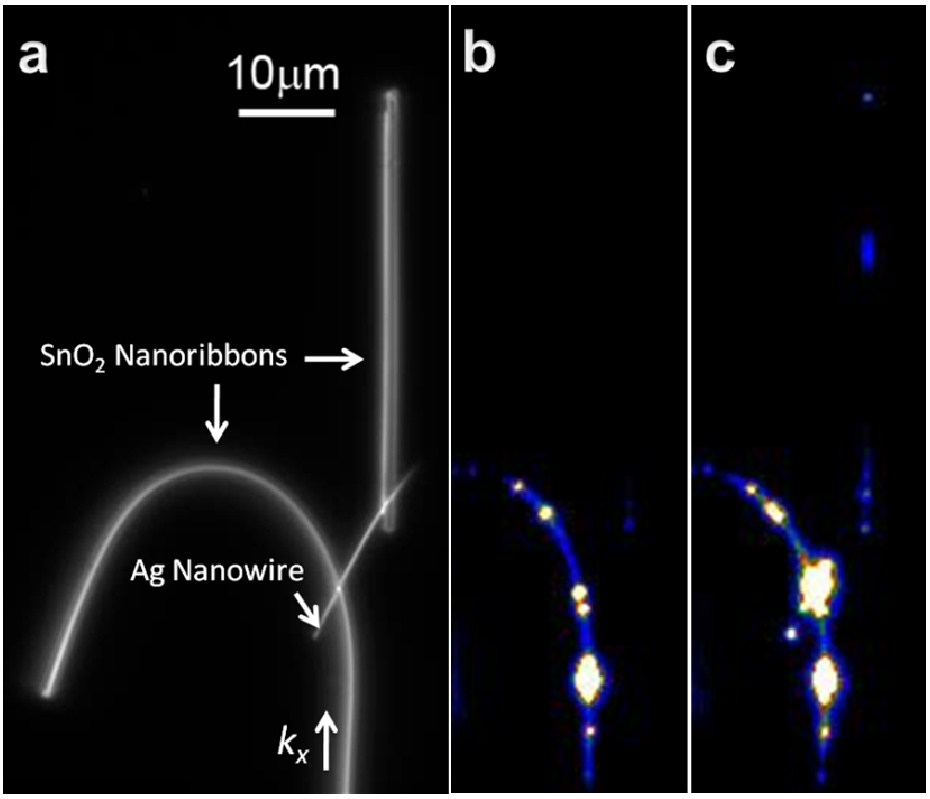

Figure 5 Dielectric-metal-Dielectric (D-M-D) optical routing circuit. a, Dark field optical image of the D-M-D coupling device, showing two SnO_2 nanoribbon bridged by a silver nanowire. **b,** Optical image of the intensity map of the device in the absence of the bridging Ag nanowire when the PL of the bent SnO_2 nanoribbon was excited from the bottom end (excitation spot not shown). No signal from the vertical ribbon was observed. **c,** Optical image of the intensity map of the device with the bridging Ag nanowire, showing a significant increase in the optical field in the vertical ribbon.

Supporting Information

Direct Photonic–Plasmonic Coupling and Routing in Single Nanowires

Ruoxue Yan, Peter Pausauskie, Jiaxing Huang, Peidong Yang

Department of Chemistry, University of California, Berkeley; Materials Sciences Division, Lawrence Berkeley National Laboratory, Berkeley, CA 94720

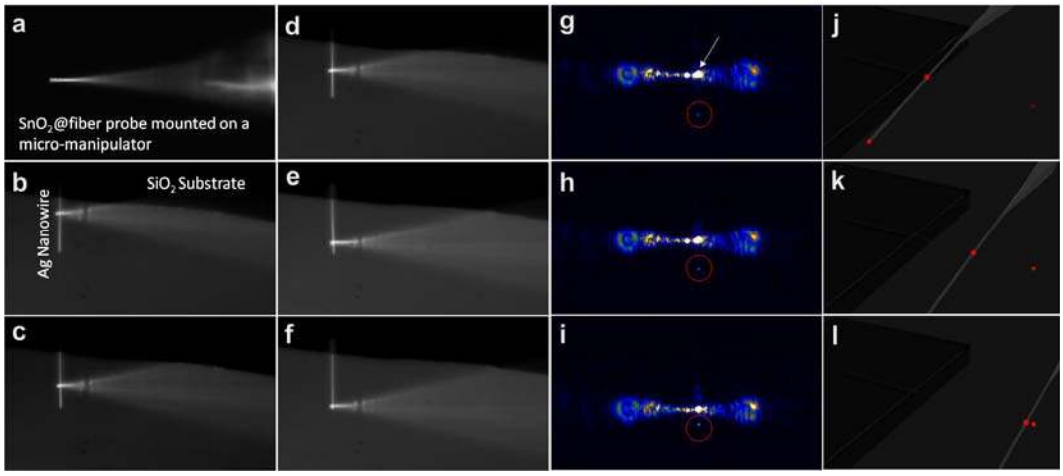

Figure S1 Optical image of the propagation loss measurement setup. a, Dark field image of the SnO_2 nanoribbon probe mounted on an x-y-z stage. The probe was ~30˚ to the focal plane of the camera. **b-f,** dark field images taken when the probe was gliding along a perpendicular silver nanowire that protrude from the edge of a SiO_2 substrate. The probe glided along the nanowire without deforming the nanowire or disturbing the coupling angle. **g-i,** Optical intensity map of the setup when the laser was coupled to the Ag nanowire through the SnO_2–Ag junction. The silver nanowire end emission intensity increased as distance of propagation decreased. **j-l,** 3D Representations of the measurement corresponding to g-l.